Available online at www.sciencedirect.com
ScienceDirect
Trans. Nonferrous Met. Soc. China 20(2010) 1331−1339
Transactions of Nonferrous Metals Society of China
www.tnmsc.cn

Applications of carbonic acid solution for developing conversion coatings on Mg alloy

YU Bing-lung(余秉隆), LIN Jun-kai(林俊凱), UAN Jun-yen(汪俊延)

Department of Materials Science and Engineering, National Chung Hsing University, 250 kuo-kuang Rd., Taichung 402, Taiwan, China

Received 23 September 2009; accepted 30 January 2010

Abstract: Works on exploring an environmentally clean method for producing an Mg,Al-hydrotalcite ($Mg_6Al_2(OH)_{16}CO_3{\cdot}4H_2O$) layer and/or calcium carbonate ($CaCO_3$) layer on Mg alloy in a carbonic acid solution system (aqueous HCO_3^-/CO_3^{2-} or Ca^{2+}/HCO_3^-) at 50 ˚C were reviewed. Conversion treatment for the Mg,Al-hydrotalcite conversion coating was as follows. Mg alloy was treated first in acidic HCO_3^-/CO_3^{2-} aqueous for precursor layer formation on Mg alloy surface and then in alkaline HCO_3^-/CO_3^{2-} aqueous to form a crystallized Mg,Al-hydrotalcite coating. Duration of an Mg,Al-hydrotalcite coating on Mg alloy surface was reduced from 12 h to 4 h by the conversion treatment. On the other hand, for reducing the formation time of $CaCO_3$ coating on Mg alloy, the aqueous Ca^{2+}/HCO_3^- with a saturated Ca^{2+} content was employed for developing a $CaCO_3$ coating on Mg alloy. A dense $CaCO_3$ coating could yield on Mg alloy surface in 2 h. Corrosion rate (corrosion current density, J_{corr}) of the Mg,Al-hydrotalcite-coated sample and $CaCO_3$-coated AZ91D sample was 7−10 μA/cm^2, roughly two orders less than the J_{corr} of the as-diecast sample (about 200 μA/cm^2). No corrosion spot on the Mg,Al-hydrotalcite-coated sample and $CaCO_3$-coated sample was observed after 72 h and 192 h salt spray test, respectively.

Key words: Mg alloy; AZ91D alloy; corrosion; conversion coating; carbonic acid

1 Introduction

Magnesium alloys have a high specific strength with a density roughly two-third that of aluminum and one-quarter that of iron[1]. These characteristics make magnesium alloys extremely attractive in vehicle applications[2−3]. However, the alloys are susceptible to corrosion in practical environments due to their high electrochemical activity[4]. Surface treatment is a basic method to improve the corrosion resistance of magnesium alloys. Many surface treatments have been adopted to increase the corrosion resistance of magnesium alloys, such as chemical conversion coating[1], anodizing[5−6], electrochemical plating[1], electroless nickel plating[7], and coating with pure magnesium by physical vapor deposition (PVD)[8−9], plasma-assisted chemical vapor deposition (PACVD)[10] as well as selected etching surface treatment[11−12]. Chemical conversion treatment is the most common surface pretreatment with low cost for improving the corrosion resistance of Mg alloys[13]. The treatment is typically based on chromate solutions[13], although hexavalent chromium is a toxic substance that pollutes environment and is detrimental to health[1]. Many studies have investigated several chrome-free conversion coating of magnesium alloys, including phosphate[14−17], phosphate-permanganate[18−19], stannate[19−23], vanadate[24], cobalt(Ⅲ) hex coordinated complex[25], cerate[26−29] or lanthanite[27] or praseodymate[27] and others. Although the above studies contributed to the substitution of Cr^{6+}-free conversion coating process, it may also have some potential risks to the environment, such as the environmental pollution of heavy metal ions and phosphorus. Moreover, the above mentioned chemical conversion coatings may make it difficult to recycle post-consumed Mg product scraps (such as from automotive components) into Mg ingots that fulfill ASTM specifications[1, 30−31]. One main reason is that impurities from the conversion coating contaminate the magnesium melt[30, 32].

In the previous study of the authors, an environmentally clean method for synthesizing a

Foundation item: Project supported by the Ministry of Education Under the ATU Plan
Corresponding author: UAN Jun-yen; Tel: +886-4-22854913; +886-4-22857017; E-mail: jyuan@dragon.nchu.edu.tw
DOI: 10.1016/S1003-6326(09)60300-9

chemical conversion coating on Mg alloys in carbonic acid solution system (aqueous HCO_3^-/CO_3^{2-} or Ca^{2+}/HCO_3^-)[33−34] was investigated. An Mg,Al-hydrotalcite ($Mg_6Al_2(OH)_{16}CO_3·4H_2O$) layer and aragonitic $CaCO_3$/Mg,Al-hydrotalcite two-layer coating was developed on AZ91D Mg alloy in an aqueous HCO_3^-/CO_3^{2-} solution and aqueous Ca^{2+}/HCO_3^- solution at 50 ˚C, respectively[33−34]. The results showed that the coatings could protect the metal substrate against corrosion. However, durations as long as at least 12 h were required to develop an aragonitic $CaCO_3$/Mg,Al-hydrotalcite or Mg,Al-hydrotalcite coating that enables to protect the Mg alloy from corrosion[33−34]. Therefore, how to shorten the treatment time to form an Mg, Al-hydrotalcite coating and/or calcium carbonate coating on AZ91D Mg alloy was also reported in our recent work. The microstructure, crystal structure and corrosion resistance of the coatings were reported.

2 Experimental

2.1 Materials

The AZ91D die-cast magnesium alloy adopted herein was the same as that used in the earlier works[8−9, 11−12, 34−35]. It has the composition (mass fraction) of 8.8% Al, 0.69% Zn, 0.212% Mn, 0.02% Si, 0.002% Cu, 0.005% Fe, 0.001% Ni and balance Mg. The original die cast plate had an area of 300 mm×240 mm and a thickness of 1.4 mm. Square coupon specimens were cut from the plate with size of 1.4 mm×20 mm×20 mm.

2.2 Preparation of Mg,Al-hydrotalcite-coated sample

AZ91D sample was ground using SiC paper (1 500 grit) and then cleaned in ethyl alcohol in an ultrasonic cleaner. HCO_3^-/CO_3^{2-} aqueous solution was prepared at room temperature by bubbling CO_2 gas through 1 000 mL of deionized water. The CO_2 gas that did not immediately dissolve in water was recycled. The recycled CO_2 gas was then recharged into the water to generate the HCO_3^-/CO_3^{2-} solution. The flow rate of CO_2 gas was 1 dm^3/min. Consequently, 20 min sufficed to minimize the pH of the solution (about 4.3). The CO_2 gas removed from industrial emissions is also believed to be able to fulfill the purpose of this work, as it is used to produce aqueous HCO_3^-/CO_3^{2-}. The carbonic acid solution was heated to 50 ˚C in a water bath. Then, six square coupons were immersed in the solution at 50 ˚C for a particular period. The immersion time changed from 1 h to 24 h. The aforementioned treatment in which samples were statically immersed in aqueous HCO_3^-/CO_3^{2-} to form a conversion layer on their surface was denoted as CO_2−A treatment, hereafter. For instant, CO_2−A−1h means that the treatment was performed for 1 h. Different treatment times are denoted similarly. AZ91D samples were immersed in HCO_3^-/CO_3^{2-} solution at 50 ˚C for 1 h (CO_2−A−1h), 2 h (CO_2−A−2h)…, 24 h (CO_2−A−24h), In another experiment, six square coupons were immersed in carbonic acid solution at 50 ˚C for 2 h while CO_2 gas was continually bubbled through the solution. The pH of the solution was kept in the range between 4 and 6. This treatment is called CO_2−B treatment. The conditions of CO_2−A and CO_2−B treatment are listed in Table 1. The pH of an HCO_3^-/CO_3^{2-} solution was increased and kept at pH 11.5 by dropwise addition of 1.25 mol/L aqueous NaOH with vigorous stirring during the mixing. The samples after CO_2−B treatment were further dipped in the pH 11.5 HCO_3^-/CO_3^{2-} solution. This treatment was denoted as, for example, CO_2−B−2h/pH11.5−2h. The notation indicates that the AZ91D sample underwent CO_2−B−2h treatment first, and then was dipped into HCO_3^-/CO_3^{2-} solution at pH 11.5 at 50 ˚C for 2 h.

Table 1 Conditions of CO_2−A[33] and CO_2−B treatment[36]

Treatment	Solution	Treating time/h
CO_2−A	Acid HCO_3^-/CO_3^{2-} solution	1−24
CO_2−B	Acid HCO_3^-/CO_3^{2-} solution with CO_2 gas continually bubbled through solution	2

2.3 Preparation of $CaCO_3$-coated sample

AZ91D samples were degreased, and then were cleaned ultrasonically in distilled water. To prepare the Ca^{2+}/HCO_3^- solution, 0.5 g and 0.7 g $CaCO_3$ powder was respectively mixed with 1 000 mL distilled water at room temperature. Experiments involved CO_2 gas bubbling through the $CaCO_3$/water slurry to dissolve the $CaCO_3$ compound. The flow rate of the CO_2 gas was the same as that used in the preparation of HCO_3^-/CO_3^{2-} aqueous solution. The CO_2 gas bubbled through the $CaCO_3$ water/slurry until the $CaCO_3$ had dissolved in water (typically taking 45 min) to yield 1 000 mL Ca^{2+}/HCO_3^- solution. The CO_2 gas not immediately dissolved in water was recycled and then recharged into the water. The solution was filtered through a filter paper before it was used for the conversion hard coating experiment. The content (mass fraction) of Ca^{2+} in the aqueous Ca^{2+}/HCO_3^- solution (0.5 g $CaCO_3$) was about 1.2×10^{-4} g/mL while that in the aqueous Ca^{2+}/HCO_3^- solution (0.7 g $CaCO_3$) was about 2.2×10^{-4} g/mL (determined by an ion-specific meter model HI 93752, HANNA instruments). Five square coupon specimens with the surfaces facing upward were statically immersed in the Ca^{2+}/HCO_3^- solution with Ca^{2+} content of 1.2×10^{-4} and 2.2×10^{-4} g/mL, respectively. The Ca^{2+}/HCO_3^- solution was heated to 50 ˚C in a water bath. The specimen immersion in the Ca^{2+}/HCO_3^- solution with Ca^{2+} content of 1.2×10^{-4} g/mL at 50 ˚C was denoted as

$CaCO_3$−treatment A. The immersion time changed from 1 h to 12 h. $CaCO_3$−A−1h means that the treatment was performed for 1 h. Similarly, AZ91D samples were immersed in Ca^{2+}/HCO_3^- solution at 50 ˚C for 1 h ($CaCO_3$−A−1h), 2 h ($CaCO_3$−A−2h), …, 12 h ($CaCO_3$−A−12h). In another experiment, five square coupon specimens with the surfaces facing upward were statically immersed in the Ca^{2+}/HCO_3^- solution with Ca^{2+} content of 2.2×10^{-4} at 50 ˚C for 2 h. This treatment is called $CaCO_3$−B treatment. The conditions of $CaCO_3$−A and $CaCO_3$−B treatment are listed in Table 2.

Table 2 Experimental conditions for $CaCO_3$−A[34] and $CaCO_3$−B treatment

Treatment	Solution	Treating time/h
$CaCO_3$−A	Aqueous Ca^{2+}/HCO_3^- solution with Ca^{2+} content of 1.2×10^{-4} g/mL	1−12
$CaCO_3$−B	Aqueous Ca^{2+}/HCO_3^- solution with Ca^{2+} content of 2.2×10^{-4} g/mL	2

2.4 Microstructure observation

Backscattered electron imaging (BEI) system in a JEOL JSM−6700F field emission scanning electron microscope (FE−SEM) was adopted to study the microstructure. The crystallographic structure of the specimens was analyzed by glancing angle X-ray diffraction (GAXRD) using Cu $K_{\alpha1}$ (1.540 5 Å) radiation.

2.5 Corrosion test

Electrochemical polarization tests and salt spray tests were employed to determine the corrosion resistance of samples. Electrochemical polarization tests were performed in a corrosion cell that contained 270 mL of 3.5% (mass fraction) NaCl solutions at room temperature at a scan rate of 0.5 mV/s. All electrochemical measurements were made using a Princeton Applied Research model 263A Potentiostat/Galvanostat and M352 software. The area of the coating exposed to the NaCl solution was 1 cm^2. Platinum gauze was used as a counter electrode and silver/silver chloride (Ag/AgCl) electrode was used as the reference. At least four experiments were performed for each experimental case. Samples were subjected to a salt spray test (ASTM B117 standard[35]). Salt spray chamber was maintained at 35 ˚C and the spray jet atomized continuously to convert salt solution into uniform small droplets.

3 Results and discussion

3.1 Reducing formation time of Mg,Al-hydrotalcite coating layer on AZ91D

In our previous study[33], CO_2−A treatment was employed to form Mg,Al-hydrotalcite layer on AZ91D sample surface. The GAXRD patterns of the samples CO_2−A−1h, CO_2−A−4h, CO_2−A−6h, CO_2−A−12h and CO_2−A−24h are presented in Fig.1. As shown in Fig.1, after treatment time of 1 h, 4 h and 6 h, weak X-ray peaks of Mg,Al-hydrotalcite were observed. Prolonging the treatment caused the GAXRD patterns to yield intense peaks of Mg,Al-hydrotalcite (JCPDS X-ray diffraction file No.22−0700). Fig.2 displays the backscattered electron images of cross-sectional microstructures of the CO_2−A sample. Fig.2(a) shows the cross-sectional microstructure of the CO_2−A−1h sample. When the immersion time was increased to 6 h (Fig.2(b)), a uniform precursor layer could be observed. Fig.2(c) displays the cross-sectional microstructure of the CO_2−A−24h sample. As indicated in Fig.2(c), the thickness of the Mg,Al-hydrotalcite layer was 5−8 μm. Fig.2(d) displays the plain-view microstructure of the CO_2−A−24h sample. Several network-like cracks at the coating layer were observed. Small cracks were distributed on the conversion coating layer during dehydration, which improved the adhesion of subsequent paint layers or organic coatings to the surface of the magnesium alloy substrate[13].

Our recent study[36] demonstrated that the formation of an Mg,Al-hydrotalcite structure on the AZ91D sample in HCO_3^-/CO_3^{2-} solution at 50 ˚C was strongly related to the pH of solution. A precursor layer of Mg,Al-hydrotalcite first covered on sample surface in acid HCO_3^-/CO_3^{2-} solution. As the CO_2−A treatment time was increased to at least 12 h, the solution turned from acidic to alkaline and the precursor layer transformed into the layer of crystalline Mg,Al-hydrotalcite[36]. The above results were exploited to shorten the time required to prepare an crystalline Mg,Al-hydrotalcite layer on AZ91D. AZ91D sample was first immersed in acidic HCO_3^-/CO_3^{2-} solution (pH 4−6) for precursor layer formation (CO_2−B) and then was

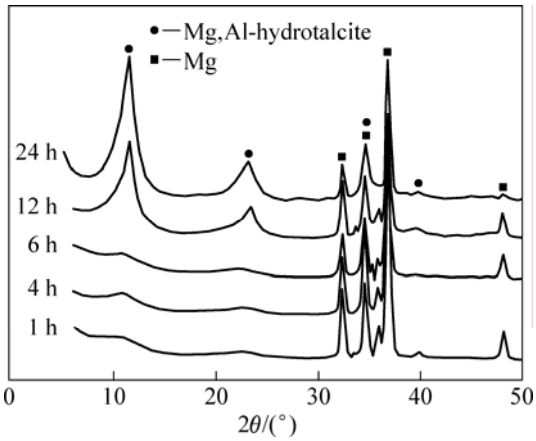

Fig.1 GAXRD patterns for sample with different CO_2−A treatment time[33]

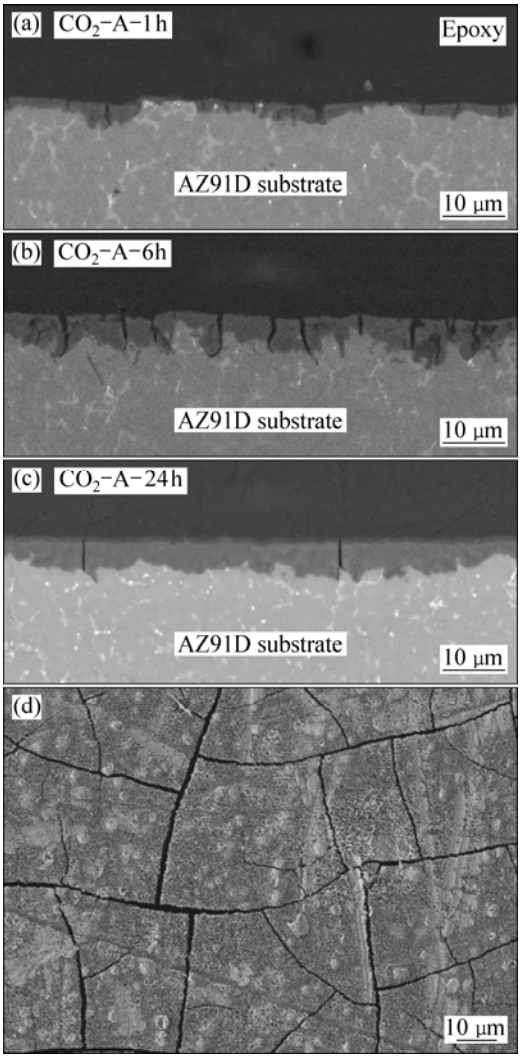

Fig.2 Cross-sectional microstructures of sample after CO_2−A treatment for different time: (a) 1 h, (b) 6 h, (c) 24 h[33]; (d) Surface morphology of sample after CO_2−A treatment for 2 h[36]

immersed in alkaline HCO_3^-/CO_3^{2-} to form crystallized Mg,Al-hydrotalcite coating. Fig.3(a) shows the GAXRD patterns of the sample after CO_2−B−2h treatment. As shown in Fig.3(a), weak and broad peaks of Mg,Al-hydrotalcite from CO_2−B−2h sample were detected, suggesting the formation of the precursor layer of Mg,Al-hydrotalcite. The GAXRD pattern of the CO_2−B−2h sample (Fig.3(a)) was similar with that of CO_2−A−1h, CO_2−A−4h and CO_2−A−6h sample (see the patterns in Fig.1). Fig.3(b) shows the cross-sectional microstructure of the CO_2−B−2h sample. As presented in Fig.3(b), a precursor layer exists on the surface of the CO_2−B−2h sample. The thickness of the Mg,Al-hydrotalcite layer was similar with that of the CO_2−A−24h sample. The samples after CO_2−B−2h treatment were subsequently immersed in an alkaline environment (pH 11.5). Fig.4 shows that the GAXRD patterns of the sample CO_2−B−2h/pH11.5−1h. The X-ray peaks of Mg,Al-hydrotalcite on the sample CO_2−B−2h/pH11.5−1h were strong (as indicated in Fig.4). Thus, the presented treatment method could be utilized to shorten the treatment time from at least 12 h to 3 h to form an crystalline Mg,Al-hydrotalcite layer on AZ91D magnesium alloy. Moreover, to form a compact Mg,Al-hydrotalcite layer, the CO_2−B−2h sample was immersed in pH 11.5 carbonic acid solution for 2 h. Fig.5(a) presents the surface microstructure of the CO_2−B−2h/pH11.5−2h sample. As indicated in Fig.5(a), this sample had crystalline Mg, Al-hydrotalcite coating layer, which, however, still exhibited several network-

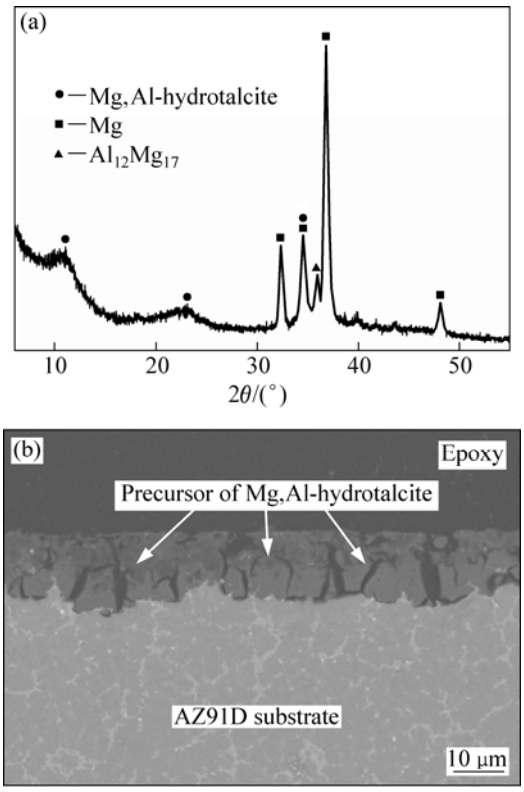

Fig.3 GAXRD pattern (a) and cross-sectional microstructure (b) of CO_2−2h sample[36]

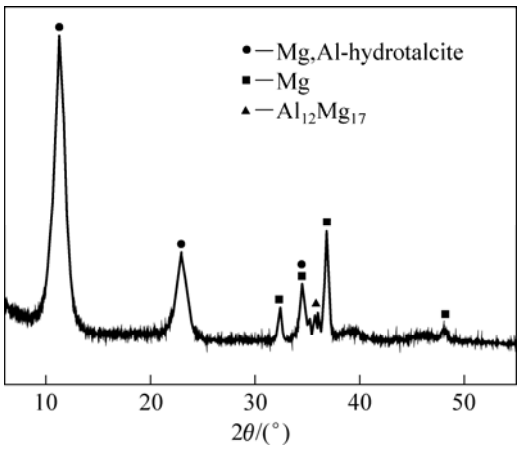

Fig.4 GAXRD pattern of CO_2−B−2h/pH11.5−1h sample[36]

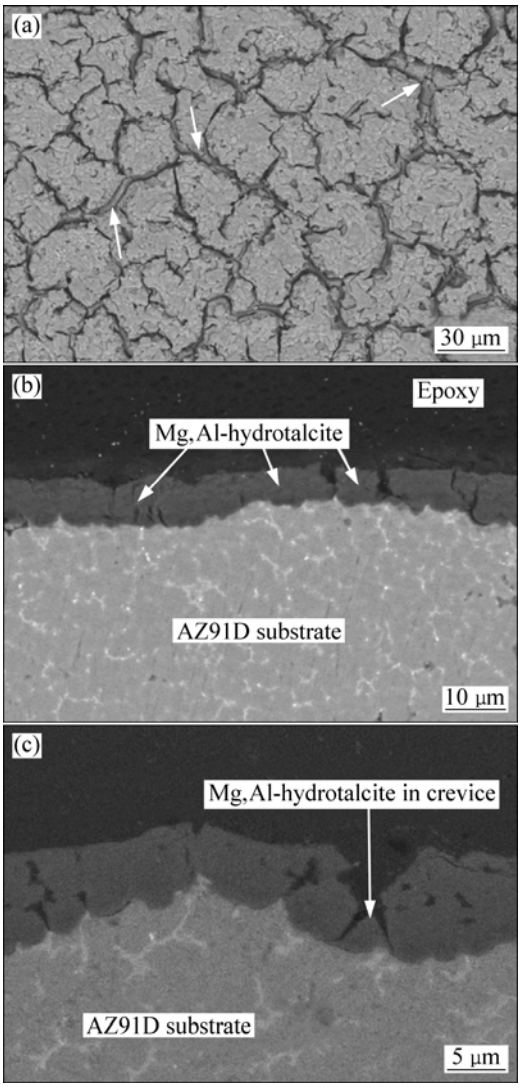

Fig.5 FE-SEM BEI images of CO_2−B−2h/pH11.5−2h sample: (a) Surface observation with arrows denoting coating materials in crevice; (b) Cross-sectional microstructure; (c) Coating material in crevice (as denoted by arrow)[36]

like cracks. The arrows in Fig.5(a) denoted that there were coating materials within the cracks. The cross-sectional microstructure of the CO_2−B−2h/pH11.5−2h was shown in Figs.5(b) and (c). The thickness of the Mg,Al-hydrotalcite layer was 5−8 μm (see Fig.5(c)). As shown in Fig.5(c), there was coating material in the crevice, avoiding the exposure of substrate metal to the environment. Hence, although the network-like cracks were observed on the coated sample surface, the crack did not penetrate the layer directly to the substrate metal.

3.2 Corrosion properties of Mg,Al-hydrotalcite conversion coating on AZ91D

The polarization curves of the samples are plotted in Fig.6. The as-cast AZ91D sample and various CO_2−2h/pH11.5-treated samples were measured in 3.5% NaCl

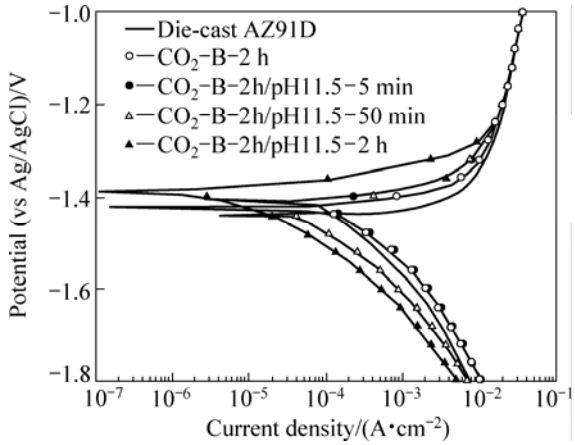

Fig.6 Polarization curves of as-cast AZ91D sample and CO_2−B−2h samples being treated in carbonic acid solution of pH 11.5 for different periods[36]

solution. The corrosion potential (φ_{corr}) of the CO_2−2h/pH11.5−2h sample was about −1.39 V (vs Ag/AgCl), while that of the as-cast AZ91D sample was around −1.45 V (vs Ag/AgCl). The AZ91D substrate had corrosion current density (J_{corr}) of about 250 μA/cm^2 and the CO_2−2h sample had J_{corr} of about 100 μA/cm^2. As shown in Fig.6, the J_{corr} of the CO_2−2h/pH11.5 samples was lower than that of the CO_2−2h sample. J_{corr} would decrease as the immersion time in pH 11.5 HCO_3^-/CO_3^{2-} solution at 50 °C increased. The J_{corr} of CO_2−2h/pH 11.5−2h sample could be down to about 10 μA/cm^2.

Therefore, the CO_2−2h/pH11.5−2h sample exhibited greater corrosion resistance than the as-cast AZ91D sample. Figs.7(a) and (b) display the surface morphologies of the samples after the salt spray test. A total 25 pieces of CO_2−2h/pH11.5−2h samples were placed in the salt spray chamber. Only two samples had small corrosion spots after 72 h of the salt spray test. Nevertheless, the surface area fraction of these corrosion spots on each of the two samples was less than 4%. Fig.7(a) shows an example of the CO_2−2h/pH11.5−2h sample surface after 72 h of the salt spray test. For comparison, as shown in Fig.7(b), the as-cast AZ91D sample was severely corroded after 12 h salt spray test.

3.3 Reducing formation time of $CaCO_3$ coating on AZ91D

Fig.8 shows the GAXRD patterns of sample after $CaCO_3$−A treatment for 10 min, 30 min, 2 h, 8 h and 12 h. The content (mass fraction) of Ca^{2+} in the aqueous Ca^{2+}/HCO_3^- solution was about 1.2×10^{-4} g/mL. The GAXRD patterns of the $CaCO_3$−A−10 min sample were composed mainly of Mg. For the sample immersed for 30 min in the Ca^{2+}/HCO_3^- solution (see Fig.8), the X-ray diffraction pattern had intensity peaks for aragonitic calcium carbonate (JCPDS cards No. 01−0628). For the

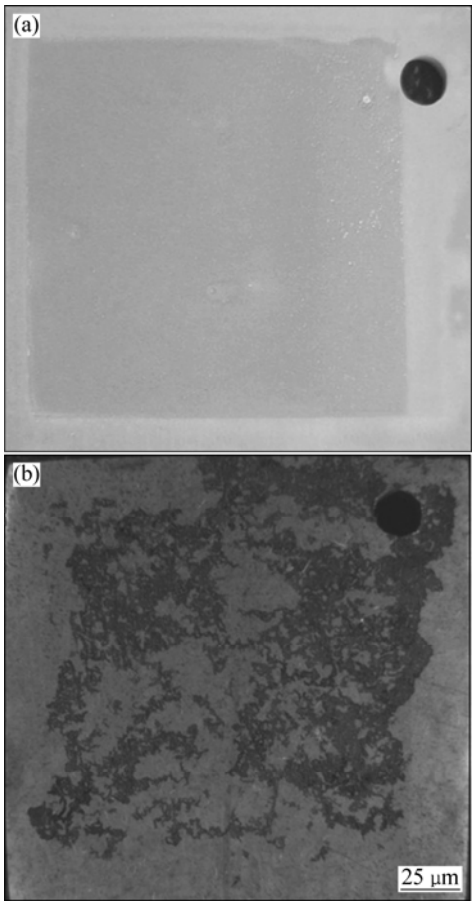

Fig.7 Surface morphologies after salt spray tests: (a) CO_2−B−2h/pH11.5−2h sample after salt spray test for 72 h; (b) As-cast sample after salt spray test for 12 h[36]

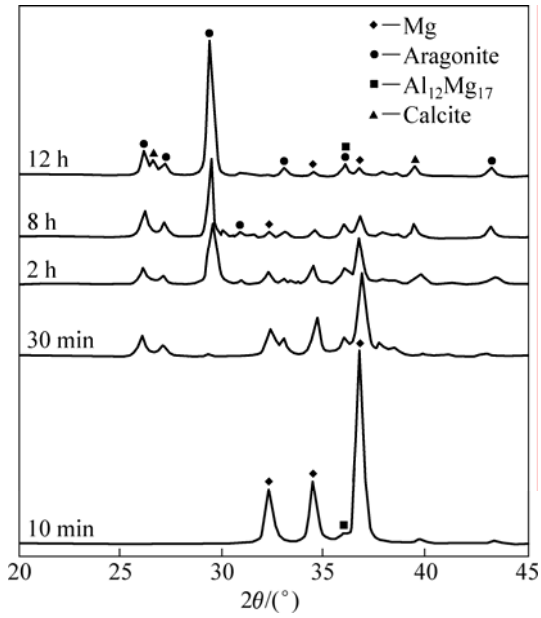

Fig.8 GAXRD patterns for sample with different $CaCO_3$−A treatment time[34]

sample immersed in the solution for 2 h, the peak of aragonite structure at a 2θ angle of 29.1° had a strong preferred orientation. The intensities of peaks at a 2θ angle of 29.1° increased as immersion duration increased (see Fig.8). Fig.9 presents the microstructures of the sample after $CaCO_3$−A treatment for 2 h and 12 h. Fig.9(a) displays the surface microstructure of the $CaCO_3$−A−2h sample. As displayed in Fig.9(a), some of the sample surface was not covered by aragonitic $CaCO_3$

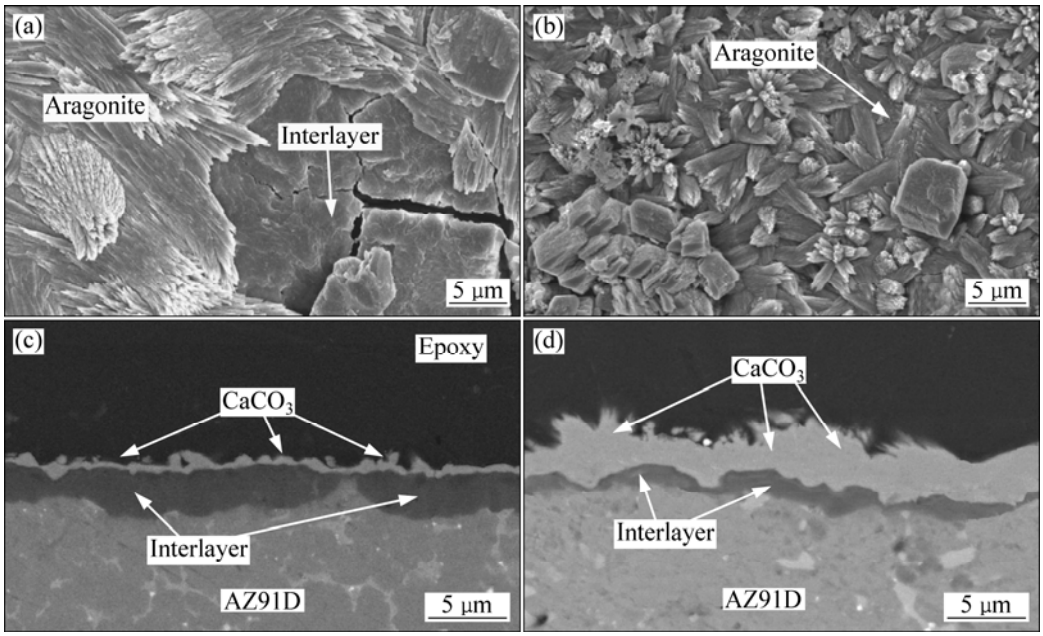

Fig.9 Microstructures of sample after $CaCO_3$−A treatment for 2 h and 12 h: (a) Surface morphology of $CaCO_3$−A−2h sample; (b) Surface morphology of $CaCO_3$−A−12h sample; (c) Cross-sectional microstructure of $CaCO_3$−A−2h sample; (d) Cross-sectional microstructure of $CaCO_3$−A−12h sample[34]

crystals. Fig.9(b) shows the surface microstructure of the $CaCO_3$−A−12h sample, indicating that the aragonitic $CaCO_3$ crystals covered the $CaCO_3$−A−12h sample surface. Figs.9(c) and (d) present the backscattered electron images of the cross-sectional microstructure of the $CaCO_3$−A−2h and $CaCO_3$−A−12h samples, respectively. As shown in Figs.9(c) and (d), the aragonite layer on $CaCO_3$−A−12h sample surface was much thicker than that on $CaCO_3$−A−2h sample surface. The thickness of aragonite layer on $CaCO_3$−A−12h sample was (3.8±0.5) μm. An interlayer was observed between aragonitic $CaCO_3$ layer and the AZ91D substrate (see Figs.9(c) and (d)). The interlayer was composed of Mg,Al-hydrotalcite structure[33]. The Mg,Al-hydrotalcite was corrosion product due to the corrosion of AZ91D substrate surface in the Ca^{2+}/HCO_3^- solution at 50 °C. Fig.10 presents the GAXRD patterns of the as-cast AZ91D sample and the sample after $CaCO_3$−B treatment for 2 h. The aqueous Ca^{2+}/HCO_3^- solution contained Ca^{2+} content up to about 2.2×10^{-4} g/mL. The diffraction patterns of the $CaCO_3$−B−2h sample showed the peaks of $CaCO_3$ (JCPDS X-ray diffraction file No. 01−0837).

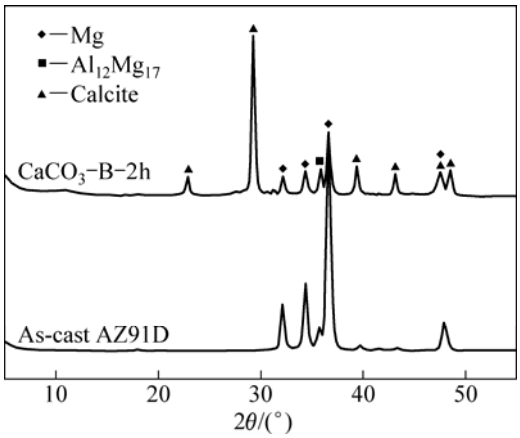

Fig.10 GAXRD patterns for as-cast AZ91D and sample after $CaCO_3$−B treatment for 2 h

Fig.11 presents the microstructure of the sample after $CaCO_3$−B treatment for 2 h. As shown in Fig.11(a), rhombohedra-shaped calcite crystals were covered on the sample surface. Fig.11(b) presents the backscattered electron images of the cross-sectional microstructure of the $CaCO_3$−B−2h sample. An Mg,Al-hydrotalcite layer was also observed between calcite $CaCO_3$ coating and the AZ91D substrate (see Fig.11(b)). By comparing the surface microstructures between the samples after $CaCO_3$−A treatment and $CaCO_3$−B treatment, it was found that the content of Ca^{2+} can remarkably affect the polymorph form of $CaCO_3$. Moreover, only 2 h for $CaCO_3$−B treatment was needed to have a $CaCO_3$ film covering on sample surface. For comparison, much more

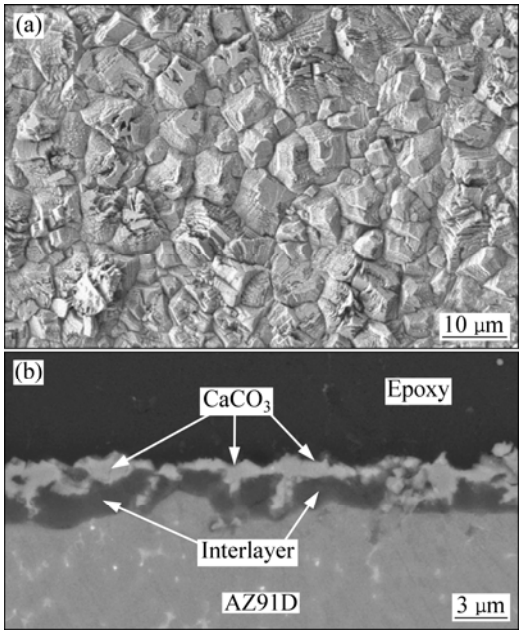

Fig.11 SEM surface morphology (a) and cross-sectional microstructure (b) of $CaCO_3$−B−2 h sample

than 2 h was needed for $CaCO_3$−A treatment to have a continuous $CaCO_3$ coating on the Mg sample. The mechanism for the formation of aragonitic $CaCO_3$ coating or calcite $CaCO_3$ coating was proposed in our previous work[34]. However, the reason that Ca^{2+} content effectively changes the polymorph of $CaCO_3$ on Mg alloy remains unclear.

3.4 Corrosion properties of $CaCO_3$ coating on AZ91D

The electrochemical test results of samples are compared in Fig.12. Corrosion potential (φ_{corr}) of the AZ91D substrate was about −1.45 V (vs Ag/AgCl). The $CaCO_3$−A−12h and $CaCO_3$−B−2h sample remained at the same level as the AZ91D substrate. The AZ91D substrate had corrosion current density (J_{corr}) of about

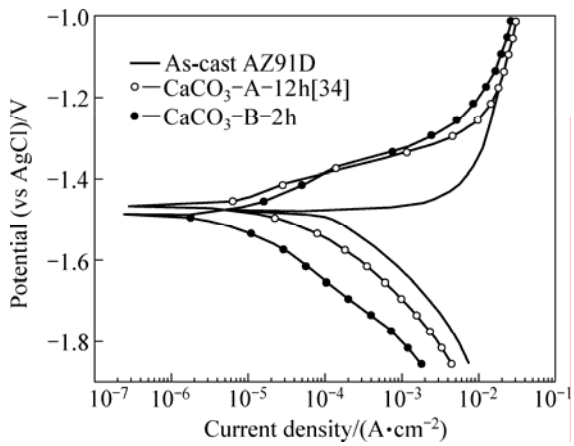

Fig.12 Polarization curves for as-cast AZ91D, $CaCO_3$−A−12 h and $CaCO_3$−B−2 h samples

250 μA/cm^2 while the J_{corr} of the $CaCO_3$−B−2 h sample was reduced to about 7 μA/cm^2. The J_{corr} of the $CaCO_3$−A−12h sample was higher than that of the $CaCO_3$−B−2h sample, suggesting that the $CaCO_3$ coating on $CaCO_3$−B−2h sample was denser than $CaCO_3$ coating on $CaCO_3$−A−12h sample surface. Fig.13 displays the surface morphologies for the samples after the salt spray test. Fig.13(a) shows that no corrosion spot was observed on $CaCO_3$−A−12h sample after 43 h salt spray test. As indicated in Fig.13(b), corrosion spot was absent on the $CaCO_3$−B−2h sample surface after 192 h of the salt spray test. Therefore, calcite $CaCO_3$ coating ($CaCO_3$−B−2h) protected the Mg alloy from corrosion in a relatively longer time than the aragonitic $CaCO_3$ coating did after $CaCO_3$−A treatment.

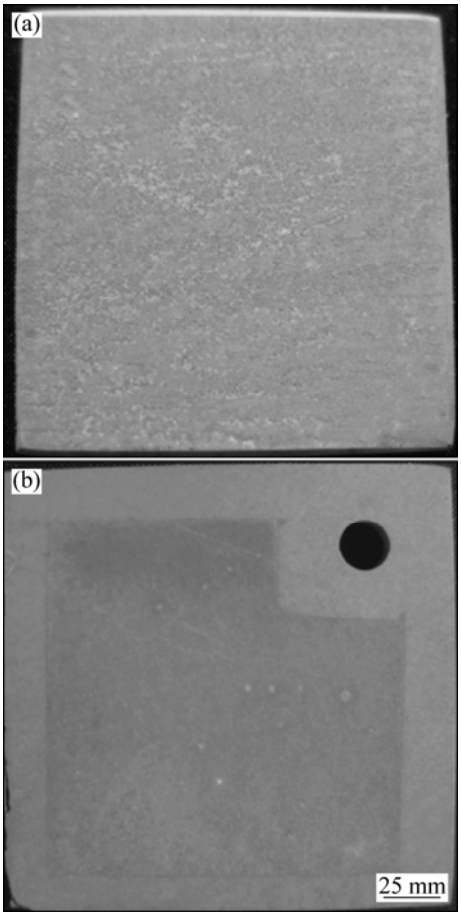

Fig.13 Surface morphologies on sample surface after salt spray test: (a) $CaCO_3$−A−12 h sample after 48 h test; (b) $CaCO_3$−B−2h sample after 192 h test

4 Conclusions

1) An environmentally clean method was explored to develop an Mg,Al-hydrotalcite ($Mg_6Al_2(OH)_{16}$-$CO_3 \cdot 4H_2O$) layer and/or calcium carbonate ($CaCO_3$) layer on Mg alloy for improving corrosion resistance of the alloy in NaCl environment.

2) To reduce the process time of developing Mg,Al-hydrotalcite conversion coating, an AZ91D sample must first be treated in an acidic HCO_3^-/CO_3^{2-} bath for precursor layer formation, and then in an alkaline HCO_3^-/CO_3^{2-} bath to form crystallized Mg,Al-hydrotalcite coating. The treatment time could be reduced to 4 h. The AZ91D sample with the crystalline Mg,Al-hydrotalcite conversion coating had nobler φ_{corr} (−1.39 V (vs Ag/AgCl)) than that of substrate AZ91D (−1.45 V (vs Ag/AgCl)). The J_{corr} of the AZ91D sample with the crystalline Mg,Al-hydrotalcite conversion coating (about 10 μA/cm^2) was evidently lower than that of the substrate metal (about 250 μA/cm^2). No corrosion spot on the crystalline Mg,Al-hydrotalcite-coated sample was observed after a 72 h salt spray test.

3) The aqueous Ca^{2+}/HCO_3^{2-} with a saturated Ca^{2+} content was employed for rapidly developing a $CaCO_3$ coating on Mg alloy. A calcite $CaCO_3$/Mg,Al-hydrotalcite coating could yield on Mg alloy surface in 2 h. The J_{corr} of the sample with $CaCO_3$/Mg,Al-hydrotalcite coating could be down to about 7 μA/cm^2. Corrosion spot on the calcite $CaCO_3$/Mg,Al-hydrotalcite coating was absent after a 192 h salt spray test.

4) The content of Ca^{2+} can affect the polymorph form of $CaCO_3$. The aragonitic $CaCO_3$ layer formed on sample surface in aqueous Ca^{2+}/HCO_3^- solution with Ca^{2+} content of about 1.2×10^{-4} g/mL while the calcite $CaCO_3$ layer formed on sample surface in aqueous Ca^{2+}/HCO_3^- solution when the aqueous Ca^{2+}/HCO_3^- solution with Ca^{2+} content up to about 2.2×10^{-4} g/mL.

References

[1] GRAY J E, LUAN B. Protective coatings on magnesium and its alloys—A critical review [J]. J Alloy Compd, 2002, 336(1/2): 88−113.

[2] BALLERINI G, BARDI U, LAVACCHI A, MIGLIORINI D, DANIELE B, BIGNUCOLO R, CERAOLO G. Magnesium alloys for structural automotive applications [J]. Magnesium Industry, 2002, 3: 16−20.

[3] SONG G, ATRENS A, JOHN D S, WU X, NAIRN J. The anodic dissolution of magnesium in chloride and sulphate solution [J]. Corro Sci, 1997, 39 (10/11): 1981−2004.

[4] JONES D A. Principles and prevention of corrosion [M]. Second Edition. Prentice Hall, Englewood Cliffs, NJ, 1996: 40−74.

[5] SHI Z, SONG G, ATRENS A. Influence of the β phase on the corrosion performance of anodized coating on magnesium-aluminium alloys [J]. Corro Sci, 2005, 47(11): 2760−2777.

[6] SHI Z, SONG G, ATRENS A. Influence of anodising current on the corrosion resistance of anodised AZ91D magnesium alloy [J]. Corro Sci, 2006, 48(8): 1939−1959.

[7] CHEONG W J, LUAN B L, SHOESMITH D W. Protective coating on Mg AZ91D alloy—The effect of electroless nickel (EN) bath stabilizers on corrosion behavior of Ni-P deposit [J]. Corro Sci, 2007, 49(4): 1777−1798.

[8] YU B L, UAN J Y. Sacrificial Mg film anode for cathodic protection of die cast Mg-9%Al-1%Zn alloy in NaCl aqueous solution [J]. Scr Mater, 2006, 54(7): 1253−1257.

[9] YU B L, UAN J Y. Sacrificial magnesium film anode for cathodic protection of die casting AZ91D alloy[C]//Magnesium Technology 2006. San Antonio, 2006: 299−304.

[10] RIE K T, WOHLE J. Plasma-CVD of TiCN and ZrCN films on light metals [J]. Surf Coat Technol, 1999, 112(1/3): 226−229.

[11] LI C F, UAN J Y. Selected etching surface treatment for improving the corrosion resistance of die cast AZ91D thin plate[C]// Magnesium Technology 2006. San Antonio, 2006: 305−310.

[12] UAN J Y, LI C F, YU B L. Characterization and improvement in the corrosion performance of a hot-chamber diecast Mg alloy thin plate by the removal of interdendritic phases at the die chill layer [J]. Metall Mater Trans A, 2008, 39(3): 703−715.

[13] AVEDESIAN M M, BAKER H. Magnesium and magnesium alloys [M]. ASM Specialty Handbook, 1999: 1−71, 143.

[14] LIN C S, LEE C Y, LI W C, CHEN Y S, FANG G N. Formation of phosphate/permanganate conversion coating on AZ31 magnesium alloy [J]. J Electrochem Soc, 2006, 153(3): B90−B96.

[15] KOUISNI L, AZZI M, ZERTOUBI M, DALARD F, MAXIMOVITCH S. Phosphate coatings on magnesium alloy AM60. Part 1: Study of the formation and the growth of zinc phosphate films [J]. Surf Coat Technol, 2004, 185(1): 58−67.

[16] ZHOU W, SHAN D, HAN E H, KE W. Structure and formation mechanism of phosphate conversion coating on die-cast AZ91D. magnesium alloy [J]. Corro Sci, 2008, 50(2): 329−337.

[17] SONG Y, SHAN D, CHEN R, ZHANG F, HAN E H. Formation mechanism of phosphate conversion film on Mg-8.8Li alloy [J]. Corro Sci, 2009, 51(5): 62−69.

[18] HAWKE D, ALBRIGHT D L. A phosphate-permanganate conversion coating for magnesium [J]. Metal Finishing, 1995, 93(10): 34−38.

[19] ZUCCHI F, FRIGNANI A, GRASSI V, TRABANELLI G, MONTICELLI C. Stannate and permanganate conversion coatings on AZ31 magnesium alloy [J]. Corro Sci, 2007, 49(12): 4542−4552.

[20] HUO H, LI Y, WANG F. Corrosion of AZ91D magnesium alloy with a chemical conversion coating and electroless nickel layer [J]. Corro Sci, 2004, 46(6): 1467−1477.

[21] GONZALEZ-NUNEZ M A, NUNEZ-LOPEZ C A, SKELDON P, THOMPSON G E, KARIMZADEH H, P LYON, WILKS T E. A non-chromate conversion coating for magnesium alloys and magnesium-based metal matrix composite [J]. Corro Sci, 1995, 37(11): 1763−1772.

[22] ANICAI L, MASI R, SANTAMARIA M, QUARTO F D. A photoelectrochemical investigation of conversion coatings on Mg substrates [J]. Corro Sci, 2005, 47(12): 2883−2900.

[23] LIN C S, LIN H C, LIN K M, LAI W C. Formation and properties of stannate conversion coatings on AZ61 magnesium alloys [J]. Corro Sci, 2006, 48(1): 93−109.

[24] YANG K H, GER M D, HWU W H, SUNG Y, LIU Y C. Study of vanadium-based chemical conversion coating on the corrosion resistance of magnesium alloy [J]. Mater Chem Phys, 2007, 101(2/3): 480−485.

[25] KIM S J, ZHOU Y, ICHINO R, RYOICHI O, MASAZUMI T S. Characterization of the chemical conversion films that form on Mg-Al alloy in colloidal silica solution [J]. Met Mater Int, 2003, 9(2): 207−213.

[26] ARDELEAN H, FRATEUR I, MARCUS P. Corrosion protection of magnesium alloys by cerium, zirconium and niobium-bath conversion coatings [J]. Corro Sci, 2008, 50(7): 1907−1918.

[27] RUDD A L, BRESLIN C B, MANSFELD F. The corrosion protection afforded by rare earth conversion coatings applied to magnesium [J]. Corro Sci, 2000, 42(2): 275−288.

[28] BRUNELLI K, DABALA M, CALLIARI I, MAGRINI M. Effect of HCl pre-treatment on corrosion resistance of cerium-based conversion coatings on magnesium and magnesium alloys [J]. Corro Sci, 2005, 47(4): 989−1000.

[29] ZHONG X, LI Q, HU J, LU Y. Characterization and corrosion studies of ceria thin film based on fluorinated AZ91D magnesium alloy [J]. Corro Sci, 2008, 50(8): 2304−2309.

[30] HANKO G, ANTREKOWITSCH H, EBNER P. Recycling automotive magnesium scrap [J]. JOM, 2002, 54(2): 51−54.

[31] JAVAID A, ESSADIQI E, BELL S, DAVIS B. Literature review on magnesium recycling[C]//Magnesium Technology 2006. San Antonio, 2006: 7−12.

[32] SKAR J I, SIVERTSEN L K, OSTER J M[C]// ICEPAM-international Conference on Environmental Friendly Pre-treatment for Aluminum and Other Metals. Oslo, 2004: 1−4.

[33] LIN J K, HSIA C L, UAN J Y. Characterization of Mg,Al-hydrotalcite conversion film on Mg alloy and Cl^- and CO_3^{2-} anion-exchangeability of the film in a corrosive environment [J]. Scr Mater, 2007, 56(11): 927−930.

[34] UAN J Y, YU B L, PAN X L. Morphological and microstructural characterization of the aragonitic $CaCO_3$/Mg,Al-hydrotalcite coating on Mg-9 wt pct Al-1 wt pct Zn alloy to protect against corrosion [J]. Metall Mater Trans A, 2008, 39(13): 3233−3245.

[35] ASTM Method B117. Standard test method of salt spray testing [S]. ASTM, Philadelphia, PA, 1990.

[36] LIN J K, UAN J Y. Formation of Mg,Al-hydrotalcite conversion coating on Mg alloy in aqueous HCO_3^-/CO_3^{2-} and corresponding protection against corrosion by the coating [J]. Corros Sci, 2009 51(5): 1181−1188.

(Edited by YANG Bing)